A Study of Measured, Experimental, and Nuclear Data Uncertainties for Subcritical Benchmark Experiments

J. Hutchinson, T. Cutler, T. Grove, M. Smith-Nelson, R. Bahran

Los Alamos National Laboratory, P.O. Box 1663 P365, Los, Alamos, NM 87545
jesson@lanl.gov

Abstract – *Recent subcritical benchmark evaluations include measured and experimental (typically systematic) uncertainties for system leakage multiplication. This work develops a methodology to also include uncertainties associated with the nuclear data which is used to infer leakage multiplication (the moments of the distribution of the number of neutrons emitted per fission, P_v).*

I. INTRODUCTION

Subcritical multiplication experiments and simulations are important for a variety of applications including nonproliferation, safeguards, and criticality safety monitoring. In recent years, LANL has designed and performed several subcritical benchmark experiments [1-3]. Part of this work included an effort to understand uncertainties associated with subcritical measurements. An approach [4-5] to estimate the statistical uncertainties on three parameters was developed based upon the Hage-Cifarelli formalism [6] of the Feynman Variance-to-Mean method [7]. The benchmark evaluations extended this to include experimental (mostly systematic) uncertainties using the same method as in critical experiment evaluations [1-2]. This work extends the methodology to include uncertainties in nuclear data used in inferring leakage multiplication (in particular the first and second moment of the P_v distribution).

II. BACKGROUND

Prompt neutrons that are produced from fission are born immediately after the fission event (on a scale of 10^{-13} or 10^{-14} seconds) and are therefore correlated in time. Recording time information about detected neutron events can be used to determine characteristics of the system being measured. Many different time-correlated methods have been used since the 1950s and are still widely utilized today [8-9].

In recent years, LANL performed subcritical experiments which included the measured (statistical) uncertainties for three benchmark parameters: detector singles count rate (R_1) i.e. the count rate in the detector system; the doubles count rate (R_2) i.e. the rate in the detector system in which two neutrons from the same fission chain are detected; and the leakage multiplication (M_L) i.e. the number of neutrons escaping a system per starter neutron. This methodology has been previously documented [4-5]. This work will focus on leakage multiplication results.

The benchmark evaluations themselves estimate the experimental (systematic) uncertainties associated with each experiment. This includes all uncertainties associated with the experiment (such as nuclear material mass, isotopics, detector placement, etc.). This is achieved via simulations using a standard sensitivity/uncertainty approach [10].

The benchmark evaluations do not include uncertainties in the nuclear data used to infer leakage multiplication. This is because nuclear data uncertainties are not included in measurement or experimental uncertainties in benchmark evaluations (for example, a critical benchmark would never have an uncertainty for any particular cross-section). Including nuclear data uncertainties is the focus of this work.

III. METHODOLOGY

1. Measured and nuclear data uncertainties

Reference 6 provides the Hage-Cifarelli equations which relate the singles (R_1) and doubles (R_2) counting rates to leakage multiplication (M_L), spontaneous fission rate (F_S), (α,n) neutron emission rate (S_α), and detector efficiency (ε).

$$R_1 = \varepsilon\left[b_{11}F_S + b_{12}S_\alpha\right]$$
$$R_2 = \varepsilon^2\left[b_{21}F_S + b_{22}S_\alpha\right]$$
$$with$$
$$b_{11} = M_L \bar{v}_{S(1)} \qquad (1)$$
$$b_{21} = M_L^2\left[\bar{v}_{S(2)} + \frac{M_L-1}{\bar{v}_{I(1)}-1}\bar{v}_{S(1)}\bar{v}_{I(2)}\right]$$
$$b_{12} = M_L$$
$$b_{22} = M_L^2\frac{M_L-1}{\bar{v}_{I(1)}-1}\bar{v}_{I(2)}$$

The terms $\bar{v}_{S(1)}$, $\bar{v}_{S(2)}$, $\bar{v}_{I(1)}$, and $\bar{v}_{I(2)}$ are the first and second factorial moments of the P_v distribution where S refers to the isotope producing spontaneous fission neutrons and I refers to the isotope undergoing induced fission. These are defined by:

$$\overline{\nu}_{(1)} = \sum \nu P_\nu \tag{2}$$

$$\overline{\nu}_{(2)} = \frac{1}{2} \sum \nu(\nu - 1) P_\nu \tag{3}$$

where ν is the number of neutrons emitted per fission with probability P_ν. These distributions depend upon the isotope that undergoes fission. For induced fission the probability distribution depends upon the energy of the neutrons that caused the fission events.

The singles and doubles counting rates are obtained by constructing Feynman histograms; the moments of these histograms are used to determine the value and uncertainty of R_1 and R_2. Previous work document the equations used to calculate these parameters [4-5].

If one assumes that starter neutrons in a system are purely from spontaneous fission, then one can set S_α to zero and Eq. 1 becomes:

$$R_1 = \varepsilon b_{11} F_S$$
$$R_2 = \varepsilon^2 b_{21} F_S$$
$$with \tag{4}$$
$$b_{11} = M_L \overline{\nu}_{S(1)}$$
$$b_{21} = M_L^2 \left[\overline{\nu}_{S(2)} + \frac{M_L - 1}{\overline{\nu}_{I(1)} - 1} \overline{\nu}_{S(1)} \overline{\nu}_{I(2)} \right]$$

Several approaches can be used to solve the Hage-Cifarelli equations. If (α, n) is set to zero, there are three unknowns in Eq. 4: the detector efficiency, spontaneous fission rate of the system, and leakage multiplication of the system. The triples counting rates could be used to have an additional equation to solve for these unknowns. Assumptions can also be used to plug in "known" values for any of the parameters and solve for the others. In this particular work, values will be plugged in for ε and the singles and doubles counting rates will be used to solve for the leakage multiplication and spontaneous fission rate.

There are several possible techniques to determine the efficiency of a detector system; this work will utilize ^{252}Cf source measurements. For ^{252}Cf measurements it is assumed that $S_\alpha = 0$ and $M_L = 1$. This reduces equation 4 to:

$$R_1 = \varepsilon \overline{\nu}_{S(1)} F_S \tag{5}$$

One can rearrange and solve for efficiency:

$$\varepsilon = \frac{R_1}{F_S \overline{\nu}_{S(1)}} \tag{6}$$

Since the terms in this equation are uncorrelated, one simply uses a quadratic sum of the derivatives to solve for the efficiency uncertainty:

$$\delta \varepsilon = \varepsilon \sqrt{\frac{\delta R_1^2}{R_1^2} + \frac{\delta F_S^2}{F_S^2} + \frac{\delta \overline{\nu}_{S(1)}^2}{\overline{\nu}_{S(1)}^2}} \tag{7}$$

Here, δR_1 is a statistical uncertainty and the uncertainty in F_S is given by a ^{252}Cf source certificate. Previous work [4-5] assumed $\delta \overline{\nu}_{S(1)}$ was 0 because nuclear data uncertainties are not included in measurement or experimental uncertainties in benchmark evaluations. The value and uncertainty of $\overline{\nu}_{S(1)}$ will be discussed in the following sections.

Once the efficiency and corresponding uncertainty are determined, one can proceed to solve for leakage multiplication using Eq. 4. Rearranging and substitution in Eq. 4 results in the quadratic equation:

$$0 = C_1 M_L^2 + C_2 M_L + C_3$$
$$with$$
$$C_1 = \frac{\overline{\nu}_{S(1)} \overline{\nu}_{I(2)}}{\overline{\nu}_{I(1)} - 1} \tag{8}$$
$$C_2 = \overline{\nu}_{S(2)} - \frac{\overline{\nu}_{S(1)} \overline{\nu}_{I(2)}}{\overline{\nu}_{I(1)} - 1}$$
$$C_3 = -\frac{R_2(\tau) \overline{\nu}_{S(1)}}{R_1(\tau) \varepsilon}$$

This quadratic equation can be solved to determine leakage multiplication:

$$M_L = \frac{-C_2 + \sqrt{C_2^2 - 4C_1 C_3}}{2C_1} = \frac{-C_2 + C_4}{2C_1}$$
$$with \tag{9}$$
$$C_4 = \sqrt{C_2^2 - 4C_1 C_3}$$

The uncertainty in leakage multiplication is:

$$\delta M_L = \sqrt{S^T Cov S} \tag{10}$$

with a sensitivity vector of:

$$S = \begin{pmatrix} \dfrac{\partial M_L}{\partial R_1} \\[2mm] \dfrac{\partial M_L}{\partial R_2} \\[2mm] \dfrac{\partial M_L}{\partial \varepsilon} \\[2mm] \dfrac{\partial M_L}{\partial \overline{v}_{S(1)}} \\[2mm] \dfrac{\partial M_L}{\partial \overline{v}_{S(2)}} \\[2mm] \dfrac{\partial M_L}{\partial \overline{v}_{I(1)}} \\[2mm] \dfrac{\partial M_L}{\partial \overline{v}_{I(2)}} \end{pmatrix} \qquad (11)$$

and a covariance matrix given in Eq. 12 at the bottom of the page. Note that previous work did not include uncertainties associated with $\overline{v}_{S(1)}, \overline{v}_{S(2)}, \overline{v}_{I(1)}$, and $\overline{v}_{I(2)}$.

The partial derivatives in Eq. 11 are:

$$\frac{\partial M_L}{\partial R_1} = \frac{C_3}{R_1 C_4} \qquad (13)$$

$$\frac{\partial M_L}{\partial R_2} = -\frac{C_3}{R_2 C_4} \qquad (14)$$

$$\frac{\partial M_L}{\partial \varepsilon} = \frac{C_3}{\varepsilon C_4} \qquad (15)$$

$$\frac{\partial M_L}{\partial \overline{v}_{S(1)}} = \frac{1}{2\overline{v}_{S(1)}}\left(1 - \frac{C_2 + 4C_3}{C_4} - 2M_L\right) \qquad (16)$$

$$\frac{\partial M_L}{\partial \overline{v}_{S(2)}} = -\frac{M_L}{C_4} \qquad (17)$$

$$\frac{\partial M_L}{\partial \overline{v}_{I(1)}} = \frac{M_L}{C_4\left(\overline{v}_{I(1)} - 1\right)}\left(C_4 + \frac{C_3}{M_L} - C_1\right) \qquad (18)$$

$$\frac{\partial M_L}{\partial \overline{v}_{I(2)}} = \frac{M_L}{C_4 \overline{v}_{I(2)}}\left(C_1 - \frac{C_3}{M_L} - C_4\right) \qquad (19)$$

The covariance term between the singles and doubles counting rates in Eq. 12 is calculated using the moments of the Feynman histograms which is described in a previous work [4-5].

The covariance between the reduced first and second factorial moments of the P_v distribution for a single isotope can be found by applying Eq. 2-3 to the standard covariance equation:

$$Cov(\overline{v}_{(1)}, \overline{v}_{(2)}) = 3\overline{v}_{(3)} + 2\overline{v}_{(2)} - \overline{v}_{(1)}\overline{v}_{(2)} \qquad (20)$$

Application of this equation, however, is not useful because the moments of the P_v distribution are directly measured (not the probabilities). For that reason, this equation cannot be used for this work as it would give covariance values that are unrealistically high. For this work, it is assumed that the covariance associated with all nuclear data terms is equal to zero. This simplifies the covariance matrix to that of Eq. 21 on the following page. In the future this covariance will be further investigated.

2. Experimental uncertainties

Experimental uncertainties are determined in the same manner as critical experiment evaluations in the ICSBEP handbook. Individual benchmark evaluations estimate the experimental uncertainties associated with each configuration. These are typically systematic uncertainties. They include all uncertainties associated with the experiment (such as nuclear material mass, isotopics, detector placement, etc.). This is achieved via simulations using a standard sensitivity/uncertainty approach [10].

$$Cov = \begin{pmatrix} \delta R_1^2 & Cov(R_1, R_2) & 0 & 0 & 0 & 0 & 0 \\ Cov(R_1, R_2) & \delta R_2^2 & 0 & 0 & 0 & 0 & 0 \\ 0 & 0 & \delta\varepsilon^2 & 0 & 0 & 0 & 0 \\ 0 & 0 & 0 & \delta\overline{v}_{S(1)}^2 & Cov(\overline{v}_{S(1)}, \overline{v}_{S(2)}) & Cov(\overline{v}_{S(1)}, \overline{v}_{I(1)}) & Cov(\overline{v}_{S(1)}, \overline{v}_{I(2)}) \\ 0 & 0 & 0 & Cov(\overline{v}_{S(1)}, \overline{v}_{S(2)}) & \delta\overline{v}_{S(2)}^2 & Cov(\overline{v}_{S(2)}, \overline{v}_{I(1)}) & Cov(\overline{v}_{S(2)}, \overline{v}_{I(2)}) \\ 0 & 0 & 0 & Cov(\overline{v}_{S(1)}, \overline{v}_{I(1)}) & Cov(\overline{v}_{S(2)}, \overline{v}_{I(1)}) & \delta\overline{v}_{I(1)}^2 & Cov(\overline{v}_{I(1)}, \overline{v}_{I(2)}) \\ 0 & 0 & 0 & Cov(\overline{v}_{S(1)}, \overline{v}_{I(2)}) & Cov(\overline{v}_{S(2)}, \overline{v}_{I(2)}) & Cov(\overline{v}_{I(1)}, \overline{v}_{I(2)}) & \delta\overline{v}_{I(2)}^2 \end{pmatrix} \qquad (12)$$

IV. EXPERIMENT INFORMATION

1. Experiment overview

This methodology was applied to the subcritical benchmark experiment of the BeRP ball (a 4483 g sphere of alpha-phase weapons grade plutonium) reflected by tungsten [2]. Eight configurations were measured in which the BeRP ball was surrounded by tungsten reflectors of varying thicknesses: 0.0, 0.5, 1.0, 1.5, 2.0, 2.5, 2.75, and 3.0 inches. Fig. 1 shows the 3.0 inch-thick W configuration with the top reflectors removed.

Fig. 1. 3.0 inch-thick Tungsten-Reflected Configuration with Top Reflectors Removed.

2. Detector systems

The detector setup consisted of two NPOD detectors [11], one SNAP detector [12], and a ~140% LN2-cooled HPGe detector [13] as seen in Fig. 2. The two NPOD neutron detectors were both located so that the face of the detectors were 50 cm from the center of the BeRP ball (the NPODs are the detectors on the same cart as the BeRP ball and tungsten reflectors). The SNAP neutron detector (detector behind the assembly in the background of Fig. 2) was located so that the center of the ^{3}He tube was 100 cm from the center of the BeRP ball. The HPGe gamma detector with bismuth shield was setup such that the front face of the detector was 150 cm from the center of the BeRP ball. Only the NPOD results are used in this work.
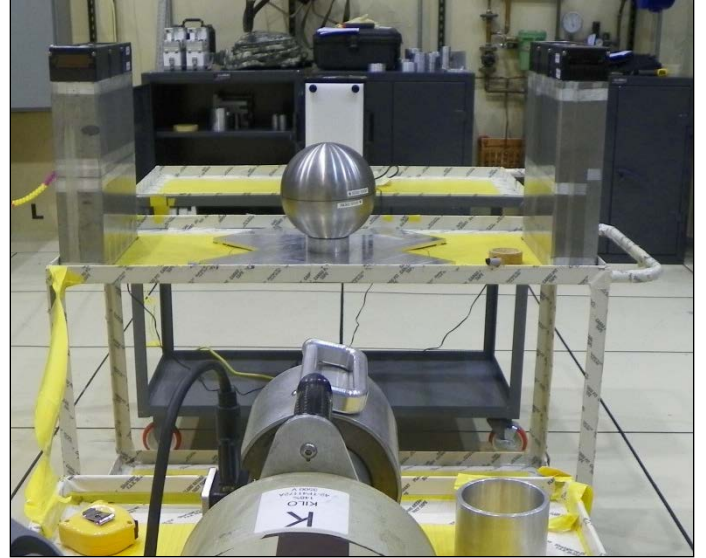

Fig. 2. 3.0 inch-thick Tungsten-Reflected Configuration.

The NPOD detectors produce list-mode data which is a time list of every neutron interaction event that was recorded in the detectors. The data produced can be analyzed using many different methods.

For the benchmark evaluation, detailed and simplified models were created. All eight configurations were modeled to include the plutonium sphere, cladding, tungsten reflectors, aluminum stand (and stand guide), aluminum base plate, all 3 carts, all 4 detector systems, and the concrete room. Fig 3 shows the MCNP®6 model for the 3.0 inch-thick W configuration. All simulations were performed using MCNP®6 [17] with ENDF/B-VII.1 [18] cross-sections. Ref. 2 includes detailed information of the measured plutonium sphere, reflectors, and detector systems.

$$Cov = \begin{pmatrix} \delta R_1^{\,2} & Cov(R_1, R_2) & 0 & 0 & 0 & 0 & 0 \\ Cov(R_1, R_2) & \delta R_2^{\,2} & 0 & 0 & 0 & 0 & 0 \\ 0 & 0 & \delta \varepsilon^2 & 0 & 0 & 0 & 0 \\ 0 & 0 & 0 & \delta \bar{v}_{S(1)}^{\,2} & 0 & 0 & 0 \\ 0 & 0 & 0 & 0 & \delta \bar{v}_{S(2)}^{\,2} & 0 & 0 \\ 0 & 0 & 0 & 0 & 0 & \delta \bar{v}_{I(1)}^{\,2} & 0 \\ 0 & 0 & 0 & 0 & 0 & 0 & \delta \bar{v}_{I(2)}^{\,2} \end{pmatrix} \quad (21)$$
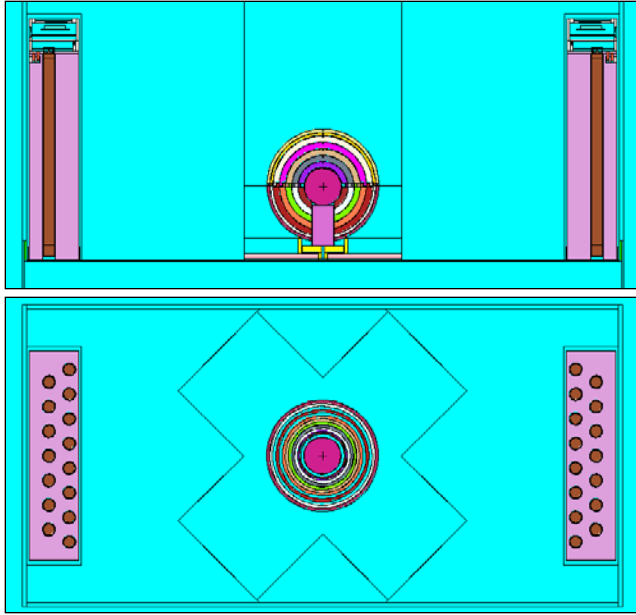
Fig. 3. 3.0 inch-thick Tungsten-Reflected Configuration (two views of NPOD detectors).

3. Nuclear data

Table 1 shows the first and second factorial moments for ^{252}Cf, ^{240}Pu, and ^{239}Pu. The ^{252}Cf and ^{240}Pu data are taken directly from published works [16-17]. For ^{239}Pu induced fission, a distribution for thermal neutron energies was first obtained. The average number of neutrons emitted, $\bar{\nu}_{I(1)}$, for fission of ^{239}Pu induced by thermal neutrons has been reported as 2.876 [16]. This cannot be directly applied to the BeRP ball measurements, since the bare BeRP ball is a fast system. An MCNP simulation of the bare BeRP ball calculated that the average neutron energy causing fission was 1.98 MeV. From ENDF/B VII.1, the average number of neutrons emitted in fission of ^{239}Pu induced by neutrons at 2 MeV is 3.178. In addition, an F4 tally multiplier was performed for fission to weight the ENDF/B VII.1 ^{239}Pu average number of neutron emitted in fission based on the energy of neutrons causing fission. This resulted in a value of 3.182 for the first factorial moment, $\bar{\nu}_{I(1)}$, shown in Table I. The second moment, $\bar{\nu}_{I(2)}$, was determined from the first moment using a data table which relates the first and second moments of the P_{ν} distribution for ^{239}Pu induced fission [18]. The uncertainty values in the moments were set so that the relative uncertainty was the same as for thermal-induced fission (a method recommended by nuclear data experts). This work assumes for the BeRP ball measurements that all spontaneous fission events occur in ^{240}Pu and all induced fission events occur in ^{239}Pu. This is a valid assumption given the isotopic content in the BeRP ball and the properties associated with these isotopes [1-2].

Table I. Factorial moments of neutron emission from fission.

Cf-252		Pu-240		Pu-239	
$\bar{\nu}_{S(1)}$	3.757 ± 0.010	$\bar{\nu}_{S(1)}$	2.154 ± 0.005	$\bar{\nu}_{I(1)}$	3.182 ± 0.010
$\bar{\nu}_{S(2)}$	5.976 ± 0.009	$\bar{\nu}_{S(2)}$	1.894 ± 0.015	$\bar{\nu}_{I(2)}$	4.098 ± 0.011

4. Experimental uncertainties

Section 2 of Ref. 2 describes the experimental uncertainties in detail. As mentioned, these are obtained by applying direct perturbation theory to simulation results. For the tungsten evaluation, 46 different parameters were included in the experimental uncertainties. For leakage multiplication, the parameters that were major contributors to the combined uncertainty included: plutonium sphere radius, tungsten shell thickness, plutonium assay (percentage of Pu inside the BeRP ball), and detector deadtime.

V. RESULTS

1. Measured and theoretical uncertainties

The measured values and uncertainties are given in Section 1 of Ref. 2 and are reproduced in Table II. They are calculated by setting the uncertainties of all of the nuclear data terms in Eq. 12 to 0.

Table II. Measured leakage multiplication values and uncertainties.

Case	Tungsten thickness (in.)	M_L	Measured uncertainty	Measured uncertainty (%)	Theoretical uncertainty (%)
1	0.0	3.371	0.030	0.90	0.88
2	0.5	4.505	0.041	0.91	0.91
3	1.0	5.770	0.053	0.92	0.92
4	1.5	7.042	0.066	0.93	0.93
5	2.0	8.391	0.079	0.94	0.94
6	2.5	9.833	0.093	0.94	0.94
7	2.75	10.483	0.099	0.94	0.94
8	3.0	11.264	0.107	0.95	0.94

It has been shown in previous work [19] that the measured uncertainty is dominated by the uncertainty of the Cf-252 source certificate (used to determine the detector efficiency in Eq. 6). An uncertainty which will be referred to here as the "theoretical" uncertainty is obtained by setting all terms in Eq. 12 to 0 except for the detector efficiency. It therefore is the minimum possible measurement uncertainty and is the uncertainty due only to the reported uncertainty in the Cf-252 source emission. Table II also includes the "theoretical" uncertainty.

2. Experimental uncertainties

The combined experimental uncertainties (calculated using a quadratic sum of the uncertainties of all evaluated experimental parameters) is given in Section 2 of Ref. 2 and is reproduced in Table III.

Table III. Leakage multiplication combined experimental uncertainty.

Case	Tungsten Thickness (in.)	Uncertainty	%
1	0.0	0.020	0.6
2	0.5	0.029	0.6
3	1.0	0.036	0.6
4	1.5	0.055	0.8
5	2.0	0.077	0.9
6	2.5	0.105	1.1
7	2.75	0.121	1.2
8	3.0	0.149	1.3

3. Nuclear data uncertainties

The nuclear data uncertainty was determined by setting $\delta R_1 = \delta R_1 = Cov(R_1(\tau), R_2(\tau)) = \delta\varepsilon = 0$ in Eq. 12 and is shown in Table IV.

Table IV. Leakage multiplication nuclear data uncertainty.

Case	Tungsten Thickness (in.)	Uncertainty	%
1	0	0.01	0.24
2	0.5	0.01	0.26
3	1	0.02	0.27
4	1.5	0.02	0.27
5	2	0.02	0.27
6	2.5	0.03	0.28
7	2.75	0.03	0.28
8	3	0.03	0.28

4. Combined uncertainties

The combined uncertainties are estimated using a quadratic sum of the measured, experimental, and nuclear data uncertainties. The combined uncertainties are shown in Table V.

Table V. Leakage multiplication combined uncertainty. Includes measured, experimental, and nuclear data uncertainties.

Case	Tungsten Thickness (in.)	Uncertainty	%
1	0.0	0.04	1.11
2	0.5	0.05	1.14
3	1.0	0.07	1.15
4	1.5	0.09	1.25
5	2.0	0.11	1.34
6	2.5	0.14	1.45
7	2.75	0.16	1.52
8	3.0	0.19	1.65

Fig. 4 shows the leakage multiplication uncertainty results. It can be seen that the uncertainties due to nuclear data are fairly small (this is the uncertainties in $\overline{V}_{S(1)}$, $\overline{V}_{S(2)}$, $\overline{V}_{I(1)}$, and $\overline{V}_{I(2)}$ only).
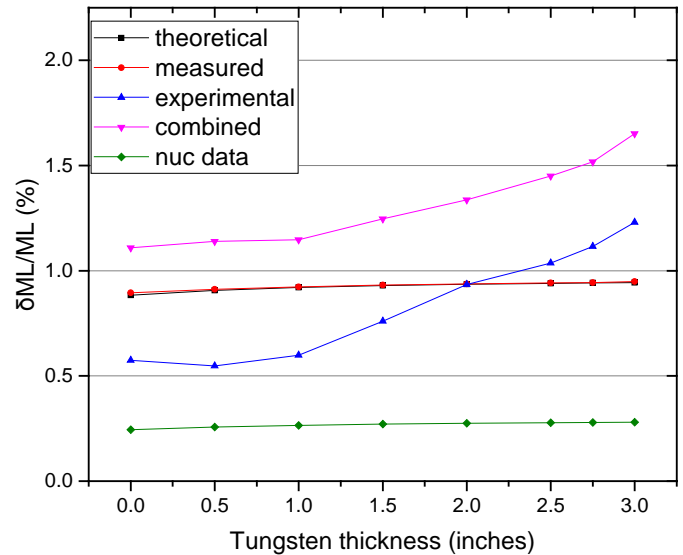

Fig. 4. Leakage multiplication (M_L) uncertainties (in %) for the BeRP ball reflected by tungsten.

Table VI gives the percentage of contribution from each source of uncertainty: measurement, experimental, and nuclear data. It can be seen from this table that the measurement uncertainties are the largest contributors to the total uncertainty when little tungsten reflection is present. For the configurations with thick tungsten reflection, however, the experimental uncertainties are larger than the measurement uncertainties. It can be seen that the percentage of contribution from nuclear data is always fairly small (2-5%) and decreases as a function of tungsten thickness; it should be noted that this uncertainty actually increases as a function of tungsten thickness, but slower

than the increase in experimental uncertainties, which results in a decrease in the percent contribution.

Table VI. Contribution (in %) of measured, experimental, and nuclear data uncertainty

Tungsten Thickness (in.)	meas %	exp %	nuc data %
0.0	65%	30%	5%
0.5	64%	31%	5%
1.0	65%	30%	5%
1.5	56%	39%	5%
2.0	49%	47%	4%
2.5	42%	54%	4%
2.75	39%	58%	3%
3.0	33%	64%	3%

VI. CONCLUSIONS

An uncertainty approach for subcritical benchmark experiments was expanded to include uncertainties associated with nuclear data used to infer leakage multiplication (the uncertainties in $\bar{v}_{S(1)}$, $\bar{v}_{S(2)}$, $\bar{v}_{I(1)}$, and $\bar{v}_{I(2)}$ only). It was shown that the nuclear data uncertainty results in only a small increase in the combined leakage multiplication uncertainty (since the contribution is smaller than the measured and experimental uncertainties).

VII. FUTURE WORK

Critical and subcritical benchmark evaluations are used for nuclear data validation. In the future, we hope to provide guidance on nuclear data evaluations (such as $\bar{v}$) using recent subcritical benchmark evaluations.

ACKNOWLEDGEMENTS

REFERENCES

1. B. RICHARD, J. HUTCHINSON, "Nickel Reflected Plutonium Metal Sphere Subcritical Measurements," International Handbook of Evaluated Criticality Safety Benchmark Experiments, NEA/NSC/DOC/(95)03/I, FUND-NCERC-PU-HE3-MULT-001 (2014).
2. B. RICHARD, et. al., "Tungsten-Reflected Plutonium-Metal-Sphere Subcritical Measurements," International Handbook of Evaluated Criticality Safety Benchmark Experiments, NEA/NSC/DOC/(95)03/I, FUND-NCERC-PU-HE3-MULT-002.
3. T. CUTLER, et. al., "IER-422: Subcritical Copper-Reflected alpha-phase Plutonium (SCRαP) Integral Experiment," Los Alamos Report LA-UR-16-26285, 2016.
4. J. HUTCHINSON, et. al., "Estimation of Uncertainties for Subcritical Benchmark Measurements," ICNC 2015, Charlotte NC, 2015.
5. J. HUTCHINSON, et. al., "Uncertainty analysis of subcritical benchmark experiments using the Hage-Cifarelli formalism," LA-UR-16-20375 (2016).
6. D. CIFARELLI, W. HAGE, "Models for a Three-Parameter Analysis of Neutron Signal Correlation Measurements for Fissile Material Assay," Nuc. Instr. Meth. A251, 550-563 (1986).
7. R. P. FEYNMAN, F. DE HOFFMANN, AND R. SERBER, "Dispersion of the Neutron Emission in U-235 Fission," J. Nucl. Energy, 64–69 (1956).
8. R. UHRIG, "*Random Noise Techniques in Nuclear Reactor Systems,*" John Wiley & Sons Inc, 1970.
9. N. PACILIO, "Reactor-Noise Analysis in the Time Domain," TID-24512, Argonne National Laboratory (1969).
10. V. DEAN, L. BLACKWOOD, "ICSBEP Guide to the Expression of Uncertainties," International Handbook of Evaluated Criticality Safety Benchmark Experiments, NEA/NSC/DOC/(95)03/I (2007).
11. C. ROMERO, "Neutron Multiplication Pod, Version 3," LANL Drawing 128Y-271079 (2001).
12. C. ROMERO, "Portable Neutron Detector SNAP 3," LANL Drawing 128Y-271264 (2004).
13. J. MATTINGLY, "Polyethylene-Reflected Plutonium Metal Sphere: Subcritical Neutron and Gamma Measurements," SAND2009-5804 (2009).
14. J. GOORLEY, et. al., "MCNP6 User's Manual," Los Alamos Report LA-CP-13-00634 (2013).
15. M. CHADWICK, et. al., "ENDF/B-VII.1 Nuclear Data for Science and Technology: Cross Sections, Covariances, Fission Product Yields and Decay Data," Nuclear Data Sheets, 112, 2887-2996 (2011).
16. P. SANTI, M. MILLER, "Reevaluation of Prompt Neutron Emission Multiplicity Distributions for Spontaneous Fission," Nuc. Sci. Eng., 160, 190 (2008).
17. N. HOLDEN, M. ZUCKER, "A Reevaluation of the Average Prompt Neutron Emission Multiplicity (Nubar) Values from Fission of Uranium and Transuranium Nuclides," BNL-NCS-35513.
18. J. LESTONE, "Energy and Isotope Dependence of Neutron Multiplicity Distributions," LA-UR-05-0288, 2005.
19. J. HUTCHINSON, "Update on Subcritical Benchmark Uncertainties," LANL report NEN-2: 16-002, LA-UR-16-20120, 2016.